

JPL Document D-75786

***TECHNOLOGY DEVELOPMENT FOR  
EXOPLANET MISSIONS***

*Technology Milestone White Paper  
Visible Nuller Coronagraph Technology Demonstration*

*Jagmit Sandhu, P.I.  
Mike Shao*

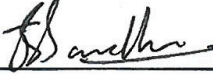
***11 March 2013***

National Aeronautics and Space Administration  
Jet Propulsion Laboratory  
California Institute of Technology  
Pasadena, California

© 2013 copyright. All rights reserved

**Approvals:**

Released by

  
\_\_\_\_\_  
Jagmit Sandhu  
Principal Investigator

5/15/13  
Date

Approved by

  
\_\_\_\_\_  
Peter Lawson  
Exoplanet Exploration Program Chief Technologist, JPL

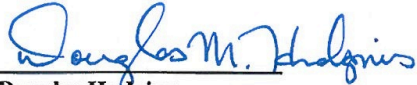
5/16/13  
Date

  
\_\_\_\_\_  
Marie Levine  
Exoplanet Exploration Program Technology Manager, JPL

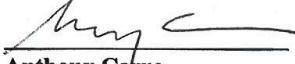
5/16/13  
Date

  
\_\_\_\_\_  
Gary Blackwood  
Exoplanet Exploration Program Manager, JPL

5/16/13  
Date

  
\_\_\_\_\_  
Douglas Hudgins  
Exoplanet Exploration Program Scientist, NASA HQ

5/17/13  
Date

  
\_\_\_\_\_  
Anthony Carro  
Exoplanet Exploration Program Executive, NASA HQ

5/17/13  
Date

# Table of Contents

<b>1. Objective</b>	<b>3</b>
<b>2. Introduction</b>	<b>3</b>
<b>2.1. Technical Approach and Methodology</b>	<b>4</b>
2.1.1 Visible Nulling Coronagraph Architecture	4
2.1.2 Speckle Suppression	8
2.1.3 APEP experiment description - current	10
2.1.4 APEP future plans	14
2.1.5 APEP path to the Milestone	15
<b>2.2. Differences Between Flight and Laboratory Demonstrations</b>	<b>18</b>
<b>3. Computation of the Metric</b>	<b>19</b>
<b>3.1. Definitions</b>	<b>19</b>
<b>3.2. Measurement of the Star Brightness</b>	<b>20</b>
<b>3.3. Measurement of the Coronagraph Contrast Field</b>	<b>20</b>
<b>3.4. Milestone Demonstration Procedure</b>	<b>21</b>
<b>4. Success Criteria</b>	<b>22</b>
<b>5. Certification</b>	<b>23</b>
<b>5.1. Milestone Certification Data Package</b>	<b>23</b>
<b>6. References</b>	<b>24</b>
<b>7. Acronyms</b>	<b>25</b>

# TDEM Milestone White Paper: Visible Nulling Coronagraph Technology

## 1. Objective

In support of NASA's Exoplanet Exploration Program (ExEP) and the ROSES Technology Development for Exoplanet Missions (TDEM), this whitepaper explains the technical approach underlying the *Visible Nulling Coronagraph (VNC) Technology Demonstration*, specifies the milestones and the methodology for computing the milestone metrics.

## 2. Introduction

TDEM Technology Milestones are intended to demonstrate significant advances in the current state of the art of extra-solar planet imaging techniques. Coronagraphs are among the key promising technologies for the detection of exoplanets. The VNC is one of the coronagraph architectures that have been extensively studied for exoplanet detection, both for ground based astronomy and space based missions. The VNC, and its close ancestor, Nulling Interferometry, have also been in development in laboratories for many years in different manifestations and wavelength ranges. Our proposal aims to demonstrate the potential of a VNC to suppress starlight to a contrast of  $3 \times 10^{-9}$ . This will be accomplished through a series of experiments using a VNC in an existing ExEP facility at JPL – the APEP testbed. We will demonstrate a progression of increasing contrast levels using laser and white light with the existing testbed. Concurrently we will design and build a wavefront sensor to achieve higher SNR wavefront control and enable post-detection speckle subtraction that will ultimately demonstrate the target contrast of  $3 \times 10^{-8}$ . Completion of this milestone is to be documented in a report by the Principal Investigator and reviewed by the Exoplanet Exploration Program.

Note: The name APEP is derived from the ancient Egyptian diety Apep – the deification of darkness and chaos, and thus the opponent of light and truth. We use the darkness/light interpretation.

This milestone reads as follows:

### **Milestone 1 definition: Narrowband Starlight Suppression with VNC**

*Demonstrate a raw coronagraph contrast of  $3 \times 10^{-8}$  (with a goal of  $3 \times 10^{-9}$ ) with the VNC at angular separations of  $2 \lambda/D$  to  $3 \lambda/D$ , using 2% bandwidth light (somewhere in the wavelength range 650 – 800 nm), for one polarization state.*

The angular separations are defined in terms of the central wavelength  $\lambda$  of the passband 650 – 800 nm, i.e. 725 nm, and the diameter  $D$  of the aperture stop as defined by the diameter of the single mode fiber array in the VNC. This demonstration will preferably be done with a pupil shear of 25% (of  $D$ ) but only if a white light source can be procured that offers sufficient brightness when expanded and sheared that the sheared pupils do not differ in intensity at any point in the pupil by more than 0.5%. Otherwise the demonstration will be done with no shear.

## 2.1. Technical Approach and Methodology

In the following sections we explain the architecture of a nulling coronagraph and our proposed wavefront sensor. We also describe the state of the APEP testbed where the experiments will be conducted.

### 2.1.1 Visible Nulling Coronagraph Architecture Nulling Interferometer

A nulling interferometer destructively interferes the light from two collecting apertures. Figure 1 illustrates the case of a two-telescope nuller. Introduction of a  $\pi$  phase shift in one arm of the interferometer (using an extra path length delay) leads to destructive interference of on-axis light. Light from an off-axis source, such as a planet, does not achieve that same  $\pi$  phase shift concurrent with the on-axis source. A subsequent imaging detector will show very little evidence of the central star but will reveal any close-by companions. A simple 2-element nuller has a sinusoidal transmission pattern on the sky:

$$T(\phi) = 1 - \cos(k\phi), \quad k = \frac{2\pi B}{\lambda}$$

$\phi$  = angular separation of the companion from star. Baseline  $B$  is the separation between the two apertures. A correct baseline length can put the planet on the first bright fringe. This fringe location corresponds to  $B = \lambda/(2\phi)$ . For an Earth-Sun system at 10 parsec,  $\phi = 0.1$  arcsec, and if observing at  $\lambda = 600$  nm, we would need  $B = 62$  cm. Therefore the configuration in figure 1 is not practical for planet detection because the separation

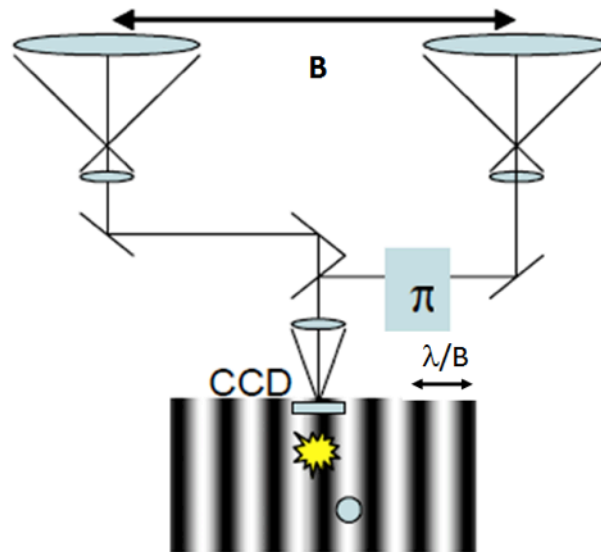


Figure 1 Schematic outline of a Nulling Interferometer, with the associated fringe transmission pattern on the sky shown below. In practice the star would be placed at the null of the fringe and the planet at the maximum.

between telescopes are rather small  $\sim 60$  cm, while the needed collecting apertures (for adequate SNR on the planet) are quite large  $\sim 4$  m. An additional problem with this setup is the need to rotate the baseline around the line of sight in order to image planets at all possible azimuthal angles.

### Nulling Coronagraph

A Nulling Coronagraph tackles these problems by using a modified Mach-Zehnder interferometer as shown in figure 2. This design splits the telescope pupil into two copies (denoted by dashed line in figure 2) and recombines them with a shear that can now be small compared to the size of the pupil. The movable rooftop optics in the two arms can be adjusted to achieve optical path length mismatching (for  $\pi$  phase shift) as well as to introduce a controlled shear between the recombined pupils, corresponding to the baseline of the interferometer. The glass plates in the two arms are used to produce an achromatic null over a useful range of wavelengths ( $\sim 20\%$  bandwidth). A second Mach-Zehnder interferometer can be used to again split and recombine the pupil with a shear in the orthogonal direction in order to obtain 2 dimensional imaging. The image obtained on a camera using the nulled output is a superposition of the nuller's sky transmission pattern on the actual image of the sky. Figure 3 illustrates the four beam null pattern obtained with an X and Y shearing nuller. A planet situated in one of the maxima lobes would be imaged while the star's light would be largely rejected if it were maintained at the minima in the center of the null pattern during observations. This is the essential architecture of some proposed NASA Astrophysics Strategic Mission Concept studies, e.g. Dilute Aperture Visible Nulling Coronagraph Imager (DAVINCI) (Shao 2009), Extrasolar Planetary Imaging Coronagraph (EPIC) (Clampin 2006), ATLAST (Postman 2009). Note that in order to map the entire field of view around a target star the 2-D transmission pattern would need to be rotated on the sky (by rotating the interferometer).

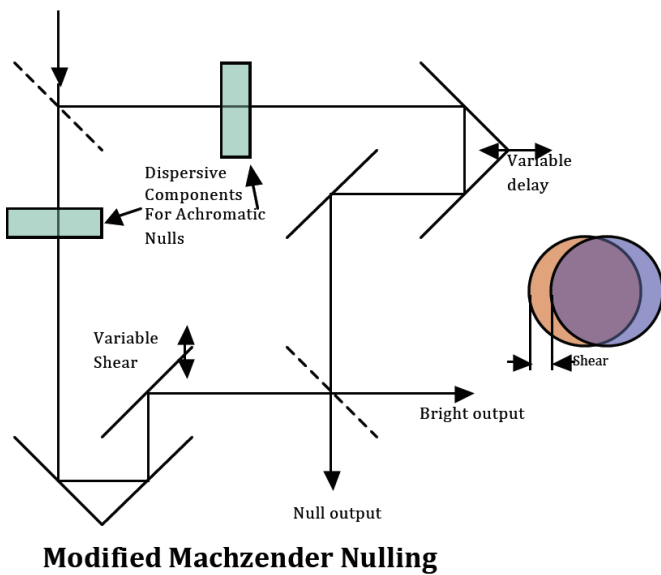


Figure 2 Schematic of a Mach-Zehnder Nuller

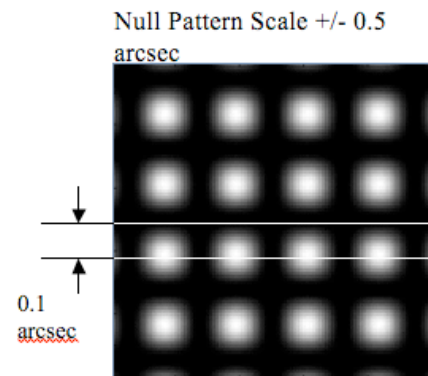


Figure 3 Transmission pattern of an X-Y shearing Nulling Coronagraph

## Control of scattered light

The null depth of a nulling coronagraph is defined as the ratio of minimum to maximum intensity of the nulled output (i.e. maximum destructive to maximum constructive interference). The null depth is a function of the phase and intensity mismatch between the two arms (Serabyn 2000):

$$N = \frac{(\Delta\theta)^2}{4} + \frac{(\Delta I)^2}{16} \quad \text{Equation 1 Null Depth of Nulling Coronagraph}$$

$\Delta\theta$  is the phase mismatch between the two arms, and  $\Delta I$  is the relative intensity mismatch of the two arms ( $I_2/I_1 - 1$ ). Figure 4 illustrates this 2-dimensional dependence of  $N$ . For example,  $N = 10^{-7}$  can be achieved with  $\Delta\theta = 50$  pm and  $\Delta I = 7 \times 10^{-4}$ .

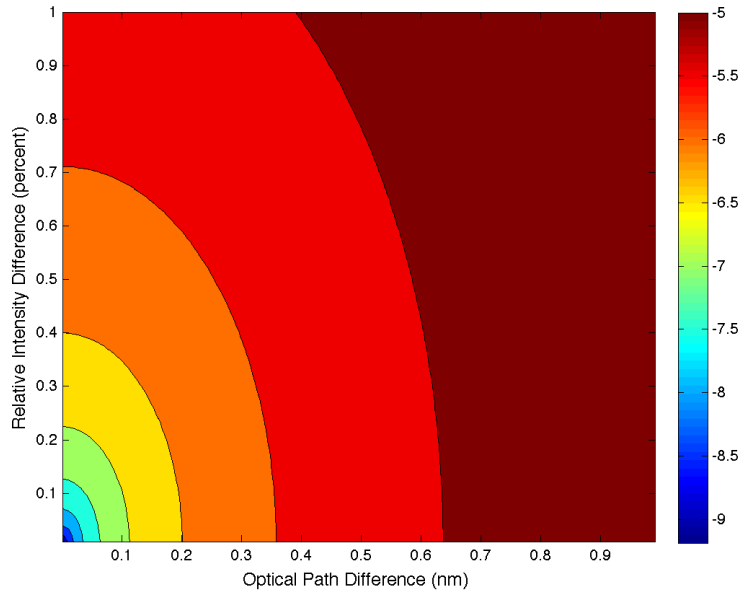


Figure 4 Null Depth as function of OPD and Relative Intensity Difference (log scale)

It is important to point out that the null depth is not the same as the contrast ratio that is of importance in planet detection and as it is written in the milestone. Contrast is a comparison of the stellar PSF peak intensity to the intensity some distance away, at a position that would be relevant for observing the planet. This separation is usually stated in units of resolution elements of the telescope,  $\lambda/D$ . Since the Airy disk PSF decreases away from the center, this position offset provides another level of rejection of starlight. The closer to the center of the PSF, the lower the rejection. Hence the challenge with building a coronagraph to work at small  $\lambda/D$ . At very high contrast levels the stellar Airy disk is replaced by speckles caused by imperfect nulling and these ultimately set the contrast floor. In our proposal we are aiming for high contrast performance at  $2 \lambda/D$  (which corresponds to a pupil shear of 25%). This separation provides a rejection factor

of at least  $5 \times 10^{-3}$  for an Airy disk. The corresponding contrast using a null depth of  $N = 10^{-7}$  is  $5 \times 10^{-10}$ . However we expect imperfections in the fiber array to limit our contrast to  $2.7 \times 10^{-9}$ .

Clearly equation 1 implies that high levels of starlight suppression require very accurate optical surfaces in both phase and amplitude. The assumption that such precise optical surfaces are available, especially for 4 m or larger sized telescopes, is not true. However there is a way to circumvent these problems. If the output of a nulling interferometer is focused onto a single mode fiber, then inside the fiber the only parameters that are important are the amplitude and phase of the electric field. If the amplitude and phase are properly matched a very deep null can be achieved. The problem has been reduced to just two degrees of freedom. But a single fiber will not provide imaging capability. To actually image an exoplanet a coherent array of single mode fibers is needed. Such an array is illustrated in figure 5.

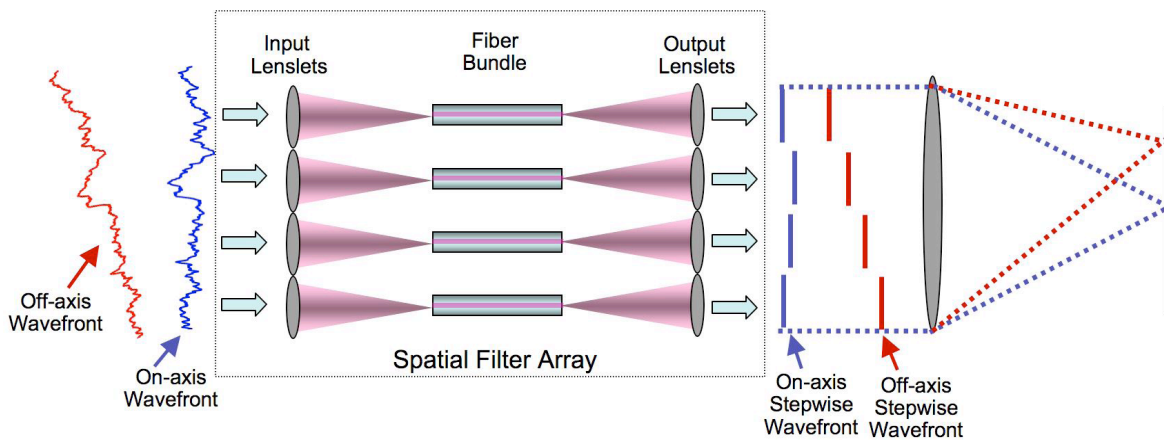


Figure 5 Principal of Spatial Filter Array. Input wavefront and amplitude aberrations are converted into intensity variations and stepwise phase on output

The pupil of the telescope would be re-imaged onto a lenslet array that focuses the light onto corresponding single mode fibers. Each single mode fiber cleans up the wavefront entering the corresponding lenslet. To achieve the phase and amplitude match required for deep nulls we need to control the tip, tilt and phase of the wavefront impinging on the input lenslet for each fiber. This is done by replacing a continuous reflective surface in one arm of the nuller with a segmented mirror. Figure 6 shows the schematic of a nuller using a segmented deformable mirror (DM). One segment of the DM maps exactly to one lenslet and fiber. With this arrangement wavefront errors at high spatial frequency, on a spatial scale smaller than a DM segment, will be filtered by the single mode fibers instead of propagating through to the science focal plane. If the optical fibers all have the same length (within  $\lambda/4$ ) the planet light from each fiber combines to form a coherent off-axis image. The phase of the residual starlight exiting the fiber array is random, hence it is scattered evenly across the whole field of view. Chopping between the two arms of the nuller gives us the intensity ratio of the two light beams for each fiber. The DM segments are then controlled in tip and tilt to vary the amount of light coupling into the fibers until the intensity of the nuller's DM arm matches that of the

reference arm. Subsequently the segments are controlled in piston only to maintain a  $\pi$  phase shift with respect to the reference arm. The pupil camera is the wavefront sensor and looks at an image of the recombined pupil. The one to one correspondence between the DM segments and the fibers along with the independence of each segment and fiber combination from all other segments and fibers naturally lends itself to wavefront sensing in the pupil plane as compared to speckle nulling in the image plane of the science camera (as is seen in some Lyot coronagraphs).

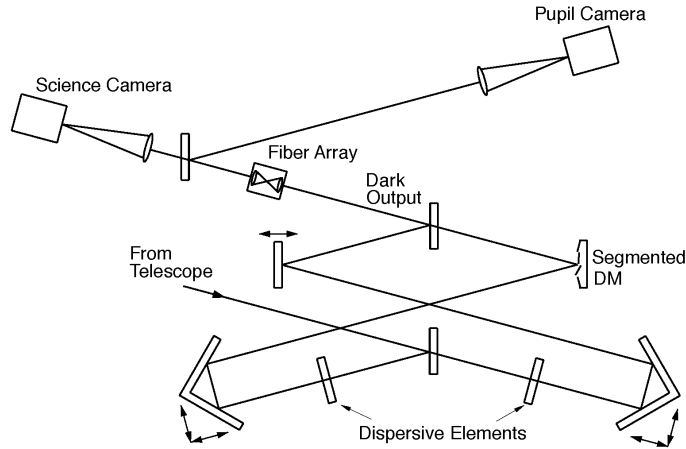


Figure 6 Schematic of Nulling Coronagraph with Fiber array and Segmented Mirror

Several investigators have implemented different versions of a nulling coronagraph. Most have been limited to single fiber experiments. Our own prior experiments with single fiber nulling have yielded suppression of laser light to  $1.25 \times 10^{-7}$  and white light (15% passband) to  $10^{-6}$  (Samuele 2007). Recently Lyon (2009) has reported narrow band nulling to  $10^{-6}$  with a 37 segment DM but without a fiber.

## 2.1.2 Speckle Suppression

The conventional wisdom is that an earth-like exoplanet can be imaged with a coronagraph that suppresses starlight to  $10^{-10}$ , about the contrast level of an exo-Earth. This nominal notion of the requirement for a coronagraph is incorrect. If the average scattered light in the coronagraph's image plane is  $10^{-10}$ , there will be 100's of speckles whose brightness is equal to that of an exo-Earth. Hence speckle suppression has to be achieved to a contrast of  $10^{-11}$  for an exo-Earth to be detected with  $< 1\%$  false alarm probability. All coronagraphs have two means of speckle suppression – optical and/or post-detection. Optical suppression attempts to prevent speckle formation via ultra-precise control of the wavefront. The fundamental limitations to active wavefront control are photon noise and the thermal stability of optics. The former needs a bright source and the latter is a challenge considering the stability required ~ even a sinusoidal ripple of 1 pm in the pupil can induce speckles of  $\sim 10^{-10}$ . Typical lab conditions are easily factors of 10-100 worse for optical path length stability. Hence optical suppression alone cannot get us to the target contrast levels of  $< 10^{-10}$ . We must combine optical speckle suppression with post-detection speckle subtraction. In this technique the speckles due to remnant

starlight are measured contemporaneously with the science image. In later data processing these speckles are subtracted from the science image, yielding the final high contrast image.

With this motivation in mind we propose to implement a post-coronagraph wavefront sensor (called the Calibrator) that utilizes both the dark and the bright outputs of the nuller, as show in Figure 7. The Calibrator serves to generate correction signals for the nuller control loop as well as measure the remnant stellar speckles for later subtraction from the science image. The idea essentially is to interfere the remnant starlight from the dark output of the nuller with a coherent reference wavefront. Additionally, with a bright reference wavefront the phase measurements can be made in a photon noise limited regime. The bright output is spatially filtered through a pinhole (diameter  $\sim 10$   $\mu\text{m}$ ) to preserve only the low order wavefront. The light in the bright output is dominated by starlight and since planet, exo-zodi and local zodi light are incoherent with starlight, the wavefront after the spatial filter is only coherent with the starlight in the dark output. A subsequent beam combiner is used to interfere the two beams. The image in the pupil camera is therefore a measurement of the starlight that leaks through the dark output.

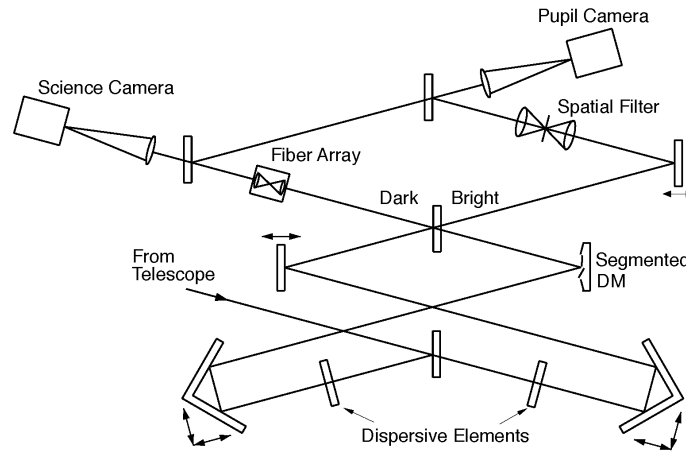


Figure 7 Schematic of Nulling Coronagraph with post-coronagraph wavefront sensor

One mirror in the reference arm is capable of precision dithering so that we can gather fringe data at two or more phase offsets. This enables calculation of the phase map and intensity, yielding the full electric field. The phase map allows generation of real time correction signals for the DM in the nuller while a Fourier transform of the electric field is equivalent to the residual speckles due to starlight leakage in the science camera (after calibration). The optical train stability requirement has thus been reduced from long term  $\sim 2$  hours per visit, to the time scale of the nuller closed loop  $\sim 60$  seconds, nearly a factor of 100.

Several authors have proposed and implemented this concept in one form or another. (Guyon 2004, Wallace et al. 2006, Vasisht et al. 2006, Rao et al. 2008). The Gemini Planet Imager will have a post-coronagraph wavefront sensor much like the calibrator outlined above (Wallace et al. 2008). A very similar sensor has been built for the P1640 coronagraph on the Palomar 5m telescope (Hinkley et al. 2011, Crepp et al. 2011, Pueyo

et al. 2012). The P1640 papers report a factor of 10 improvement in speckle suppression via post processing. These sensors were built at JPL and our team has contributed directly to these projects and is intimately familiar with the details of implementation and successful operation. Rao (2008) discuss a method whereby they use visibility data in the calibrator to generate DM correction signals since that metric is immune to exact starting phase in the calibrator. We intend to explore several algorithms that we have used in different projects where we have implemented this design. Initial results with the P1640 coronagraph using reconstruction of the PSF on Alpha Cyg have shown reduction of static speckles by a factor of  $\sim 5$  to 10 (private communication).

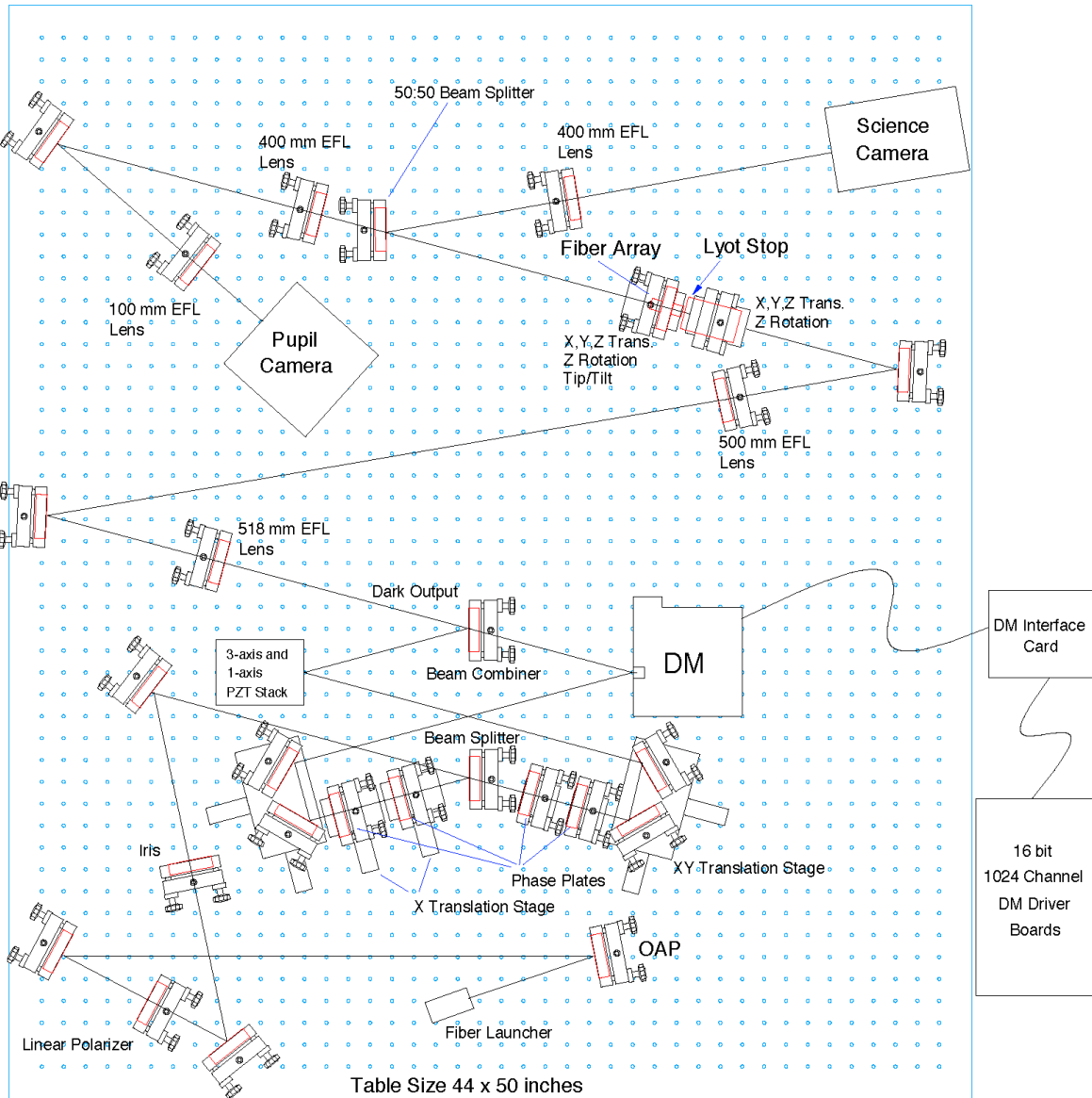
### 2.1.3 APEP experiment description - current

A nulling coronagraph requires some key optical components that are unique to this concept, namely a segmented DM and fiber array. Fortunately we will be able to leverage an existing facility that has made excellent progress in the development and integration of these new technologies into a working nuller. This is the APEP testbed at JPL. APEP was initiated as an Advanced Strategic Mission concept Study in 2008 in order to advance the state of visible nulling coronagraphy. The facility has integrated all the parts for a working nuller and recently started experiments aimed at demonstrating nulls.

Figure 8 shows the optical layout of APEP. Light launched from a single mode fiber is collimated by an off axis parabola (OAP). A linear polarizer ensures that only light with  $s$  polarization (i.e. perpendicular to the optical table surface) is launched into the nuller. Ultimately the polarizer will be removed to demonstrate simultaneous nulling in both  $s$  and  $p$  polarizations. Each arm of the nuller has a roof top mirror assembly and a carefully designed pair of glass plates of different refractive indices to enable control of dispersion. The plates have wedges such that when they are moved perpendicular to the light beam a varying amount of glass can be used to match dispersion and thereby satisfy the  $\pi$  phase shift condition over the wavelength range of 650 to 800 nm. Until now the experiments have only been done in laser light so that this dispersion matching step has not been needed.

The DM is used to control the shape of the wavefront for intensity and phase matching of the two arms of the nuller. The non-DM arm of the nuller (the ‘reference’ arm) has a flat mirror on a piston, tip and tilt mounts assembly. This mirror is used to match tip/tilt to the DM arm and also for achieving  $\pi$  optical path difference (OPD) in the nuller. During null acquisition this mirror is dithered in 4 steps of  $\pi/2$  phase shifts at the center wavelength to enable phase calculation by the real time control system using the pupil camera images. The phase values are converted to motion commands for the DM actuators and sent out to update the DM in time for the next iteration of the 4-step dither cycle. Once the null has been acquired this 4-step dither cycle is suspended so that science camera data can be collected and the null metrics measured.

The dark output of the nuller is imaged onto a Lyot Stop that blocks light corresponding to the DM segment edges and any defective DM segments. Immediately behind the Lyot stop is the single mode fiber array. The output of the fiber array is split into two beams with a beam splitter. One beam is imaged onto the science camera and the second one is imaged onto the pupil camera CCD.



APEP Optical Layout (without Calibrator)

Figure 8 Optical Layout of APEP testbed

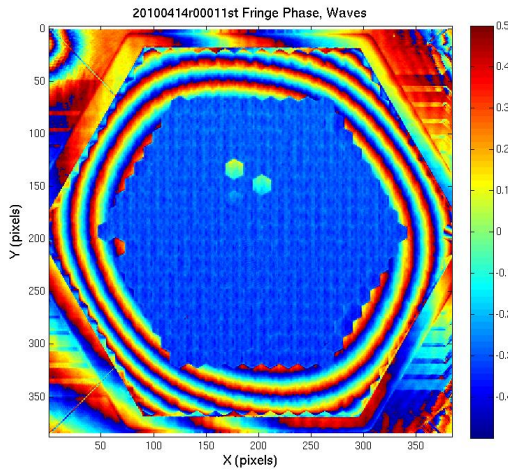


Figure 9 Phase Measurement of DM

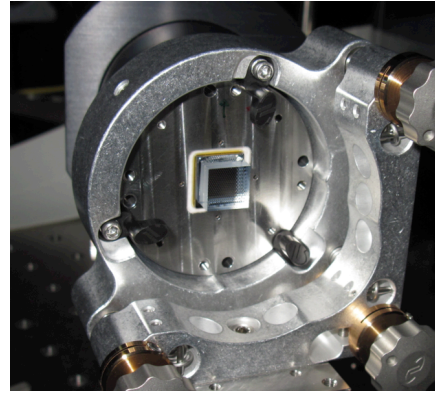


Figure 10 Output face of Fiber array

## Deformable Mirror

The DM is a gold coated 331 segment MEMS (microelectromechanical system) device manufactured by Boston Micromachines. The segments are hexagonal with 517  $\mu\text{m}$  spacing (center to center). Each segment is supported on 3 actuators thereby allowing independent control of tip, tilt and piston. Figure 9 shows a phase measurement of the DM with the central 217 segments actuated to produce a near flat wavefront. All 331 segments can be controlled but only 217 are used because the fiber array is limited to that number. Light from the unused segments is blocked by the Lyot stop. Also apparent in the image are fringes in the unused segments. These are due to curvature of the DM substrate.

The control electronics for the DM were custom built at JPL with 16 bit precision per channel. This is necessary for sub-nanometer control of the DM segment motion. After accounting for the geometric locations of the actuators and their non-linear response to the input voltage via careful calibration, the 3 actuators behind each segment can be controlled so that the segments move independently in piston, tip or tilt.

## Lyot Stop

The DM has four defective segments and the gaps between segments are 5 microns. The light from these areas of the DM and the reference arm cannot be nulled. Hence we have designed a Lyot Stop to reject the light from both arms corresponding to the defective segments and gaps. The Lyot stop consists of circular pupils (diameter 470  $\mu\text{m}$ ) for each DM segment. The circular shape matches the pupil shape of each microlens. An afocal imaging relay images the DM segments onto the Lyot Stop so that the light emerging from the Stop is collimated for optimum coupling into the fiber array.

## Fiber array

Immediately behind the Lyot Stop is the fiber array. It consists of a hexagonal packing of 217 single mode fibers with 500  $\mu\text{m}$  spacing, each about 1 cm long, with lenslets on both the input and output faces. This array was fabricated by Fiberguide industries and figure 10 shows the output side. There is a one to one correspondence between the DM segments and the fibers – i.e. light from one DM segment couples into only one fiber via its input side lens.

The light coming out of the fiber array consists of an array of 217 beams, each with an apodization corresponding to the single fundamental mode in the fiber. Figure 11 illustrates the intensity distribution and also the fact that some fibers are defective. Close inspection of the beam profiles shows that they are nearly single mode with a few exceptions due to imperfections in the lenslet fabrication and incorrect alignment of the lenslets with the fibers.

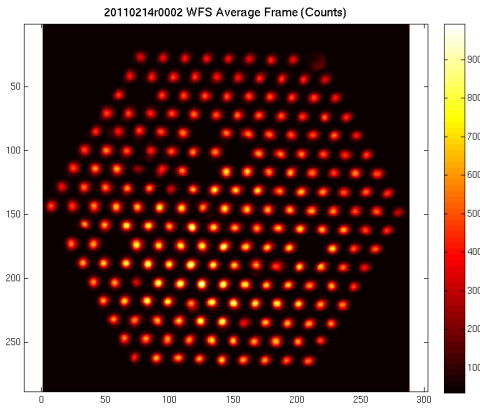


Figure 11 Intensity measurement of fiber array output beam

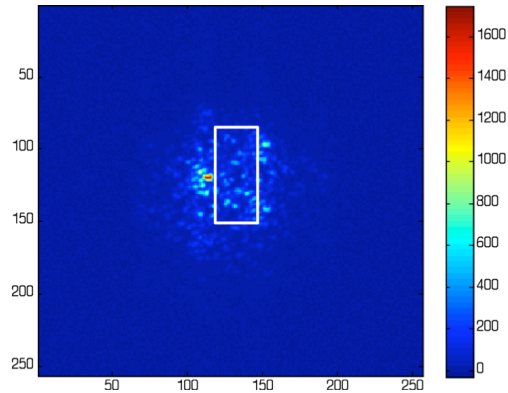


Figure 12 Science Camera Image

While figure 11 is an image taken by the wave front sensing (pupil) camera, figure 12 shows the corresponding image in the science camera. The hexagonal symmetry of the sidelobes arises from the arrangement of the fibers. Obviously the PSF is not perfect. The speckles between the PSF core and the sidelobes are due to the fiber+lenslet combinations of the fiber array not being completely coherent among all the 217 fibers. This limited coherence of the fiber array does not restrict our ability to demonstrate nulls at the required levels because our nulling algorithm uses the pupil plane data where each fiber output is sensed independently. If there were a planet in the light source the limited coherence of the fiber array would degrade the strehl ratio of its PSF and hence reduce SNR. A future generation fiber array would have to be built more precisely to preserve planet SNR.

Figure 12 also outlines a rectangular box over which we have made a preliminary measurement of our nulling performance. The box extends  $8 \lambda/D$  in X and  $24 \lambda/D$  in Y. The measured contrast is  $1.3 \times 10^{-5}$  (corresponding to a  $10^{-2}$  null). It is important to point out that this is without any intensity matching in a turbulent laboratory air environment.

## Wavefront sensing and control

The current control loop for the nuller consists of dithering the reference arm in 4 steps of  $\pi/2$  phase shifts at the laser wavelength (633 nm). Phase for each pixel is calculated. Pixels for each segment are averaged and the resulting value is fed back to the DM to move the corresponding segment in piston only. Figure 13 shows one such phase measurement illustrating the fact that phase over each lenslet is nearly single mode (the

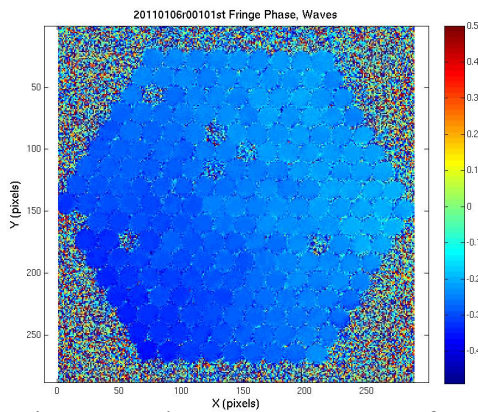


Figure 13 Phase measurement of  
fiber array output

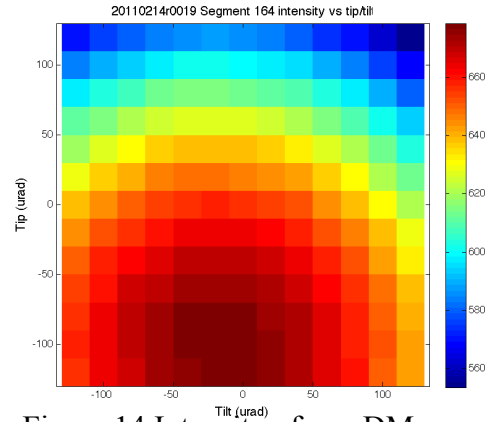


Figure 14 Intensity of one DM segment  
as a function of its tip and tilt

scale is  $\pm 0.5$  wave at 633 nm). In air the root mean square of the phase map is about 4 nm. The tip/tilt degree of freedom for each segment is only used to vary the coupling of light from a segment to the corresponding fiber. This mode of operation is still under development. Figure 14 shows preliminary data illustrating the nearly 20% intensity variation in one segment/fiber combination for a tip/tilt range of  $\pm 150$  micro radians.

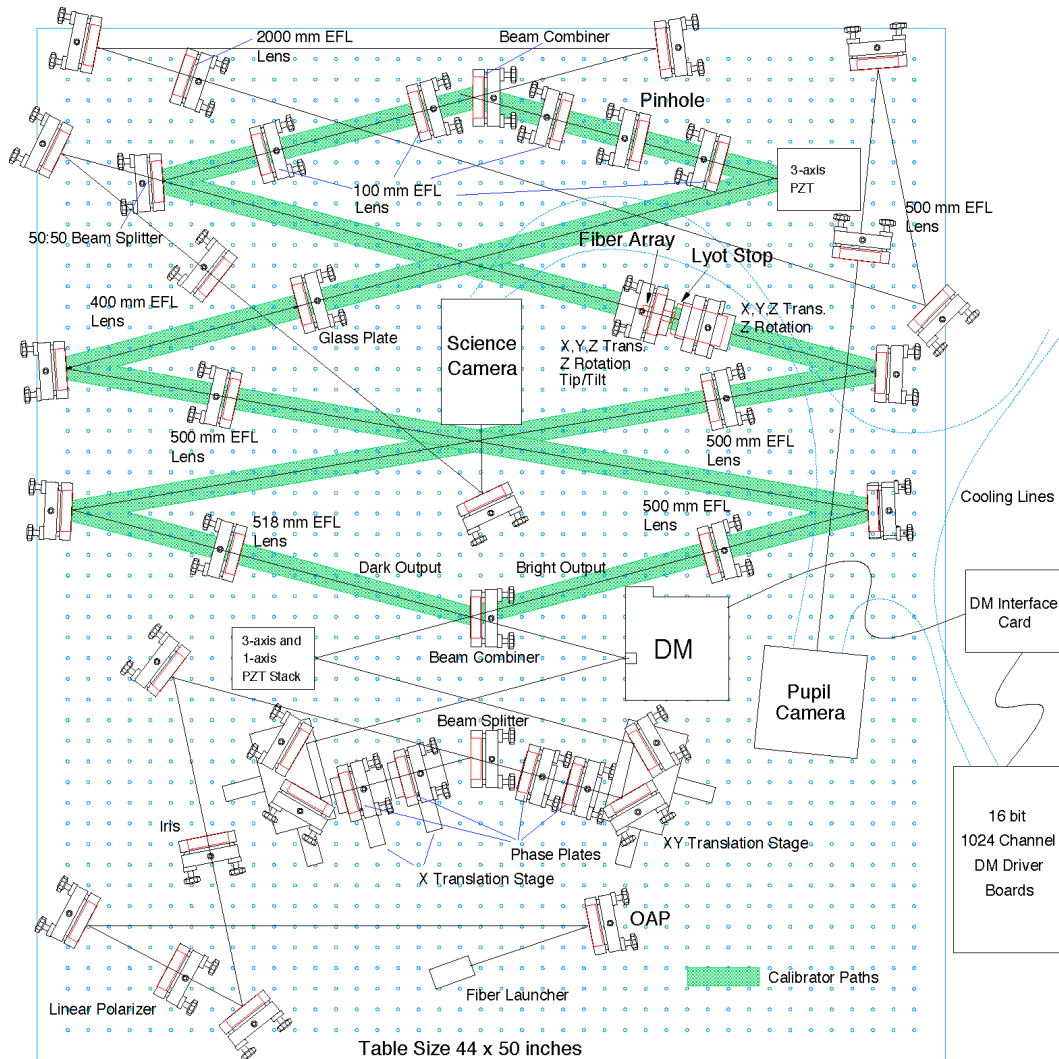
### 2.1.4 APEP future plans

In addition to continuing the VNC experiments on APEP, we propose to modify the current layout to add a post-coronagraph wavefront sensor, to support our milestone effort. Figure 15 is a tentative optical layout showing the Calibrator optical path in green. The notable items in the new layout are:

1. Glass plate in the reference arm of the Calibrator to match the dispersion due to the fibers+lenslets in the dark arm.
2. Spatial filter. This layout uses off the shelf lenses for the spatial filter needed in the reference arm of the Calibrator but we propose to use reflective OAPs in the real implementation to avoid chromatic aberrations in the lenses. The dark arm has corresponding optics for the spatial filter but no pinhole. This is to match the pupil flip that occurs in the reference arm spatial filter.
3. Imaging lenses for the pupil camera are longer focal length because it now has to image the fiber output face from a farther distance than in the current setup.
4. A piston/tip/tilt stage in the reference arm of the Calibrator. This enables tip/tilt and OPD matching to acquire fringes and also for dithering during operation for phase measurement.

- Cooling lines are attached to the science and pupil camera as well as the DM electronics chassis for thermal stability during vacuum operation.

Additionally, the real time control system would need to be augmented to enable control of both nuller and calibrator interferometers, as well as feedback of DM corrections from the calibrator to the nuller. All of the above involve standard software techniques that have been implemented in a few testbeds at JPL and do not pose a challenge.



APEP Optical Layout With Calibrator

Figure 15 APEP Optical Layout With Calibrator

### 2.1.5 APEP path to the Milestone

Previously we showed our present status of a  $10^{-2}$  null (figure 12). Past experiments with single fiber nulling have been able to achieve  $10^{-7}$  (laser) and  $10^{-6}$  (white light) nulls in air (Samuele 2007). We believe that our current null is limited by poor performance

from the fiber array. As shown in figure 4, we need  $<0.1\%$  intensity matching to obtain nulls  $< 10^{-7}$ . In our testing of the fiber array we have found that the fibers cannot match intensity better than about 5%. On close investigation we believe that this is because the lenslet+fiber+lenslet combination is not acting like a single mode fiber. Figure 16 is a plot of the ratio of intensities of the two arms of the nuller, as seen from the output side of the fiber array. Each individual circular area corresponds to light from one lenslet output. The noteworthy aspect is that the ratio within each lenslet is not uniform but has gradients of  $\pm 15\%$ . If each fiber was truly single mode the output waveform would look the same no matter which arm of the nuller was feeding light into the fibers. We suspect that the fibers insufficiently reject light in the cladding and this light manages to travel to the output side, thereby polluting the single mode wavefront which travels along the core of the fibers. This is happening despite the presence of pinholes on both the input and output fiber faces (to limit cladding light).

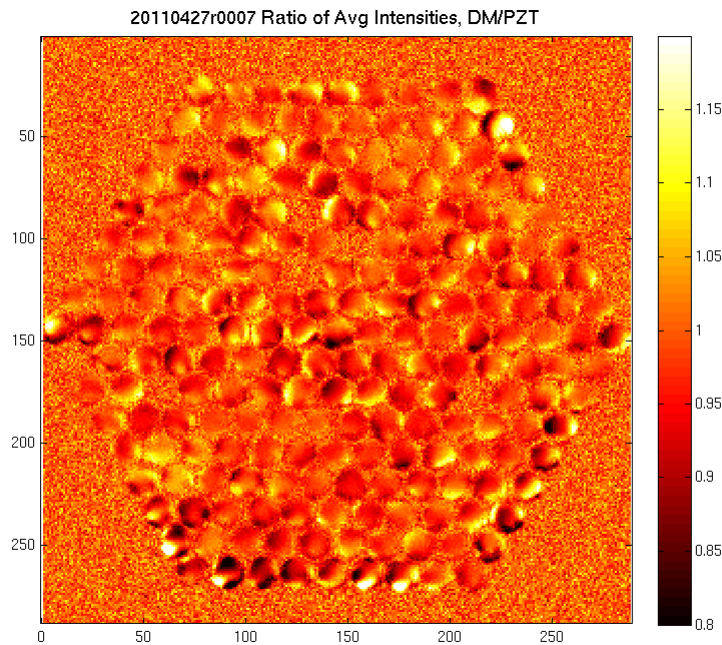


Figure 16 Ratio of intensities of two arms of nuller

The problem is compounded by the fact that the fibers are not enclosed in an index-matched medium that would allow cladding light to escape each fiber. The fibers are held in place by a series of silicon wafers with holes drilled in them, with epoxy holding the whole configuration together. Since the refractive index of the wafers and epoxy is not matched to the fibers, cladding light is able to propagate the length of the fibers due to total internal reflection. We are now experimenting with a single fiber in the lab to verify our conjectures and also to check that an index matched medium surrounding the fibers will enable the cladding light to be rejected. After this step we can finalize a design for a new fiber array that will meet the single mode criteria and allow us to intensity match at the level of  $\sim 0.1\%$  that is required for  $10^{-7}$  nulls.

Table 1 lists the progression of increasing contrast levels that we plan to demonstrate on the way to the final milestone. Note that the milestone refers to an inner working angle (IWA) of  $2 \lambda/D$ . The IWA is simply the first peak of the nuller fringe pattern on the sky =  $\lambda/2B$  ( $B$  = baseline, i.e. shear between the two arms of the nuller). Therefore  $IWA = 2\lambda/D$  implies  $B = D/4$ , where  $D$  = telescope aperture. Clearly IWA could be made smaller by increasing  $B$  but this requires nulling starlight even closer to the peak of the stellar PSF. Note that DAViNCI uses physically separate apertures while EPIC uses a single aperture telescope (with splitting and shearing) to achieve the same effect of fringes on the sky.

**Table 1.** Technical path for Demonstration of Starlight Suppression in VNC

Year	Contrast	Illumination/Bandpass	Air/Vacuum/ Speckle-subtraction
0.3	$1 \times 10^{-5}$	Laser	In Air, No speckle-subtraction
0.6	$10^{-6}$	Laser	In Air, speckle-subtraction
1.2	$3 \times 10^{-8}$	Laser	In Vacuum, New Fiber Array, with speckle-subtraction
2	$3 \times 10^{-8}$	White Light/2%	In Vacuum, New Fiber Array, with speckle-subtraction

It is important to reiterate the difference between null and contrast. Null refers to the ratio of peak stellar PSF values, while contrast refers to the ratio of peak stellar PSF to an off-axis PSF, at least  $2 \lambda/D$  away. Since there are 217 independent fibers, after nulling the remnant starlight emerging from these fibers with independent phase errors will give rise to roughly 217 independent speckles in the focal plane. Therefore if the starlight is nulled to  $10^{-5}$  then the average stellar intensity in off-axis area will be  $10^{-5}/217 \sim$  i.e.  $5 \times 10^{-8}$ . All of the contrast levels in table 1 use the fiber quantity of 217. If we had a 1000 fiber array available (as envisaged in some flight projects) we would be able to achieve improvement in contrast by another factor of 5. We expect the post-coronagraph wavefront sensor and speckle subtraction to provide an additional improvement of at least 10. These metrics underlie the progression of contrast levels shown in Table 1.

**Step 1 - Demonstrate Contrast  $< 10^{-5}$  using laser light at 633 nm in ambient air environment.**

This is the simplest experiment that allows us to debug the hardware and rapidly develop necessary algorithms for nulling and contrast measurement. The aim is to demonstrate functionality rather than performance. The contrast level to be demonstrated  $\sim 10^{-5}$ , is appropriate for an in-air environment where typical wavefront stability is  $\sim 1$ - $2$  nm rms, and the limits of our current fiber array, as underscored earlier.

**Step 2 - Demonstrate Contrast  $< 10^{-6}$  using laser light at 633 nm in ambient air environment, with post-detection speckle subtraction.**

Subsequently we will implement the post-coronagraph wavefront sensor which will enable measurement of remnant starlight and its subtraction from the science image, providing a factor of  $\sim 10$  improvement in the contrast.

**Step 3 - Demonstrate Contrast  $< 3 \times 10^{-8}$  using laser light at 633 nm in Vacuum, with post-detection speckle subtraction.**

At this time we hope to have designed and fabricated a new fiber array. We believe we can achieve  $< 1\%$  intensity matching (down from the existing array's  $\sim 15\%$ ), mainly

limited by current fabrication techniques. This predicts a null depth of  $6 \times 10^{-6}$ , corresponding to a contrast  $\sim 6 \times 10^{-6} / 217 / 10 \sim 3 \times 10^{-9}$ . This will be a significant demonstration of high contrast imaging using a VNC with a coherent fiber array.

**Milestone - Demonstrate Contrast  $< 3 \times 10^{-8}$  using white light with 2% bandpass, with post-detection speckle subtraction.**

This milestone will demonstrate our control of dispersion (with custom designed phase plates) and zero path length control in the nuller (necessary for white light interferometry).

## 2.2. Differences Between Flight and Laboratory Demonstrations

Two NASA Astrophysics Strategic Mission Concept studies have used a VNC architecture for exoplanet imaging - Dilute Aperture Visible Nulling Coronagraph Imager (DAViNCI) (Shao 2009) and the Extrasolar Planetary Imaging Coronagraph (EPIC) (Clampin 2006). A VNC has also been flown on a sounding rocket experiment and survived the crash landing (Rao 2008). DAViNCI is a phased dilute aperture telescope array with a nulling interferometer, imager, and spectrometer designed to detect and characterize extra-solar planets over the wavelength range 550 to 1700 nm. The key differences of the APEP VNC from the flight version are:

1. The flight VNC has two nullers in series. The first nulls in the X direction (on the sky) and the second in the Y direction in order to provide 2-dimensional imaging. The APEP VNC in our experiment is 1-dimensional.
2. The flight VNC will have a larger DM and fiber array  $\sim 1000$ -2000 segments/fibers, to accommodate a larger pupil and enhanced contrast ratio. The APEP DM has 331 segments and fiber array has 217 fibers due to current fabrication limitations.
3. Flight VNC will have X and Y shear to achieve sinusoidal transmission on the sky. This aspect is very difficult to replicate in the lab because of the nature of lab light sources. Typically we use a laser fed through a single mode fiber to a collimating lens/Off axis parabola to provide the light source for the nuller. The light distribution in the laser is Gaussian and remains so after collimation. In principal it is possible to use a large focal length lens/OAP to pick up the central piece of the Gaussian distribution so that the intensity fall off to the edge is  $< 1\%$ . However this comes at a significant cost to the throughput of the laser light to the nuller (since we are using a very small part of the wavefront emanating from the fiber). This problem is particularly acute for white light sources that are generally much fainter than laser sources. Hence we will likely not be able to demonstrate sheared waveform nulling. This is not a significant drawback because the rest of the nuller operation does not care whether the wavefront is sheared or not. The crucial steps of intensity and phase matching are independent of the shear.
4. Flight environment will expose the special purpose optics – DM and fiber array - to a space radiation whose effects on their performance are unknown. The expected effect on fibers is very small (from known IR fiber measurements).

## 3. Computation of the Metric

### 3.1. Definitions

The contrast metric requires a measurement of the intensity of speckles appearing within the dark field, relative to the intensity of the incident star. The contrast metric will be assessed in terms of statistical confidence to capture the impact of experimental noise and uncertainties. In the following paragraphs we define the terms involved in this process, spell out the measurement steps, and specify the data products.

**3.1.1.** “Raw” Image and “Calibrated” Image. Standard techniques for the acquisition of CCD images are used. We define a “raw” image to be the pixel-by-pixel image obtained by reading the charge from each pixel of the CCD, amplifying and sending it to an analog-to-digital converter. We define a “calibrated” image to be a raw image that has had background bias subtracted and the detector responsivity normalized by dividing by a flat-field image. Saturated images are avoided in order to avoid the confusion of CCD blooming and other potential CCD nonlinearities. All raw images are permanently archived and available for later analysis.

**3.1.2.** We define “scratch” to be a DM setting in which actuators are set to a predetermined surface figure that is approximately flat.

**3.1.3.** We define the “star” to be a point-like source with a diverging wavefront such that the collimating optics cannot resolve any structure in the source. The source in APEP uses a single mode fiber with a 4  $\mu\text{m}$  mode field diameter. The collimating optics must have an F# such that  $\lambda * F\# > 4 \mu\text{m}$  at all wavelengths in the band 650 – 800 nm.

**3.1.4.** We define the “algorithm” to be the computer code that takes as input the measured speckle field phase, and produces as output voltage values (3 per segment) to be applied to each segment of the DM, with the goal of driving the segments to the null condition.

**3.1.5.** The “contrast field” is a dimensionless map representing, for each pixel of the science camera, the ratio of its value to the value of the peak of the central PSF that would be measured in the same testbed conditions (light source, exposure time, etc.). The measurement of the central PSF peak is explained in section 3.2 while the calibration of the contrast field is further detailed in Section 3.3.

**3.1.6.** The “contrast value”,  $c$ , is a dimensionless quantity that is the average value of the contrast field over the dark field adopted for the experiment.

**3.1.7.** “Statistical Confidence”. The milestone objective is to demonstrate a mean contrast value of  $C_0 = 3 \times 10^{-9}$  with a confidence coefficient of 0.90 or better. Estimation of this statistical confidence level requires an estimation of variances. Given that the speckle fields contain a mix of static and quasi-static speckles (the residual speckle field remaining after the completion of a wavefront sensing and control cycle, speckle subtraction via the calibrator measurements, together with the effects of alignment drift following the control cycle), as well as other sources of measurement noise including photon detection statistics and CCD read noise, an analytical development of speckle statistics is impractical. Our approach is to make the full set of measurement available to enable computation of the confidence levels for other statistics. After  $n$  iterations of determining the contrast value  $c$  (as defined in 3.1.6), with  $n > 100$ , we shall report that

contrast value  $c_m$  such that 90% of value of  $c$  are  $> c_m$  . The totality of measurements will be reported to verify whether the underlying distribution is Gaussian or not.

## 3.2. Measurement of the Star Brightness

The brightness of the star is measured with the following steps.

**3.2.1.** One arm of the nuller is blocked to prevent transmission of starlight to the beam combiner. This implies that one-fourth of the input starlight will reach the science camera (one-half each is lost at the beam splitter and beam combiner).

**3.2.2.** To create the photometric reference, a representative sample of short-exposure (e.g. a few milliseconds) images of the star is taken with the science camera.

**3.2.3.** The images are averaged to produce a single star image. The “short-exposure peak value” of the star’s intensity is estimated, either the value of the maximum-brightness pixel or an interpolated value representative of the apparent peak. This value is multiplied by four to account for the light lost in the nuller (see 3.2.1).

**3.2.4.** The “peak count rate” (counts/sec) is measured for exposure times of microseconds to tens of seconds.

## 3.3. Measurement of the Coronagraph Contrast Field

Each “coronagraph contrast field” is obtained as follows:

**3.3.1.** The nuller control loop is initiated and the nuller driven to the best null position (least light output from the dark port of the nuller). The operational mode of the nuller has been explained in 1.3.1 and 1.3.2.

**3.3.2.** An image (typical exposure times are  $\sim$  tens of seconds) is taken of the coronagraph field (the suppressed star and surrounding speckle field), along with wavefront sensor data to compute the electric field of the remnant stellar light. The remnant will be subtracted from the science camera image before computation of the contrast value. Figure 17 shows the measured PSF from APEP. We have marked two circles – one at  $2 \lambda/D$  and the second one at  $8 \lambda/D$ . The outer boundary corresponds to the nyquist frequency of adjacent fibers. For the milestone the contrast value will be calculated in the region  $2-3 \lambda/D$ .

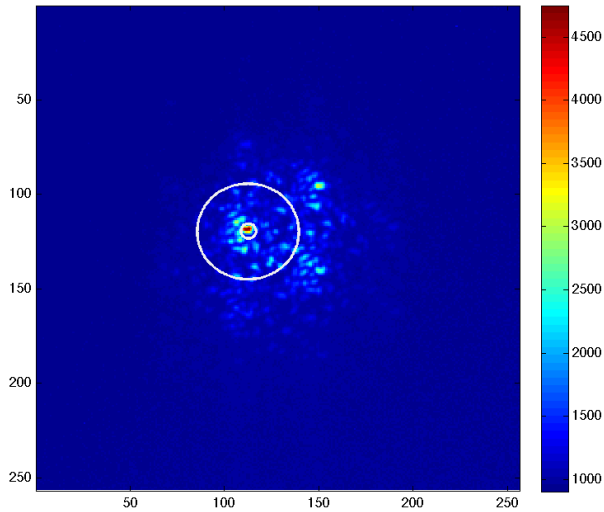


Figure 17 Annulus for computation of contrast metric

The image is normalized to the “star brightness” as defined in 3.2. The contrast field image is averaged over the target high-contrast areas, to produce the contrast value. To be explicit, the contrast value is the sum of all contrast values, computed pixel-by-pixel in the dark field area and then divided by the total number of pixels in the dark field area, without any weighting being applied. The rms contrast in a given area can also be calculated from the contrast field image.

### 3.4. Milestone Demonstration Procedure

The procedure for the milestone demonstration is as follows:

**3.4.1.** The DM is set to scratch. An initial coronagraph contrast field image is obtained as described in Sec. 3.3.

**3.4.2.** Wavefront sensing and control is performed to find settings of the DM actuators that give the required high-contrast in the target dark field. This iterative procedure may take from one to several hours, starting from scratch, if no prior information is available.

**3.4.3.** A number of contrast field images are taken, following steps 3.3.1 – 3.3.2. The result at this point is a set of contrast field images. It is required that a sufficient number of images are taken to provide statistical confidence that the milestone contrast levels have been achieved, as described in Section 3.1.7 above.

**3.4.4.** Laboratory data are archived for future reference, including raw and calibrated images of the reference star and contrast field images.

## 4. Success Criteria

The following are the required elements of the milestone demonstration.

- 4.1. Illumination is 2% bandwidth or smaller in white light in the range of  $650 \text{ nm} < \lambda < 800$  light in single polarization, .
- 4.2. A mean raw contrast metric of  $3 \times 10^{-8}$  or smaller shall be achieved in a 2 to 3  $\lambda/D$  dark zone, as defined in Sec. 3.3.2, with a goal of  $3 \times 10^{-9}$ .
- 4.3. Criterion 4.2, averaged over the data set, shall be met with a confidence of 90% or better, as defined in Sec. 3.1.7. Sufficient data must be taken to justify this statistical confidence.
- 4.4. Elements 4.1 – 4.3 must be satisfied on three separate occasions with a reset of the wavefront control system software (DM set to scratch) between each demonstration.

*Rationale: This provides evidence of the repeatability of the contrast demonstration. The wavefront control system software reset between data sets ensures that the three data sets can be considered as independent and do not represent an unusually good configuration that cannot be reproduced. For each demonstration the DM will begin from a "scratch" setting. There is no time requirement for the demonstrations, other than the time required to meet the statistics stipulated in the success criteria. There is no required interval between demonstrations; subsequent demonstrations can begin as soon as prior demonstrations have ended. There is also no requirement to turn off power, open the vacuum tank, or delete data relevant for the calibration of the DM influence function.*

## 5. Certification

The PI will assemble a milestone certification data package for review by the ExEPTAC and the ExEP program. In the event of a consensus determination that the success criteria have been met, the project will submit the findings of the review board, together with the certification data package, to NASA HQ for official certification of milestone compliance. In the event of a disagreement between the ExEP project and the ExEPTAC, NASA HQ will determine whether to accept the data package and certify compliance or request additional work.

### 5.1. Milestone Certification Data Package

The milestone certification data package will contain the following explanations, charts, and data products.

- 5.1.1.** A narrative report, including a discussion of how each element of the milestone was met, and a narrative summary of the overall milestone achievement.
- 5.1.2.** A description of the optical elements, including the fiber array, and their significant characteristics.
- 5.1.3.** A tabulation of the significant operating parameters of the apparatus.
- 5.1.4.** A calibrated image of the reference star, and the photometry method used.
- 5.1.5.** A contrast field image representative of the data set, with appropriate numerical contrast values indicated, with coordinate scales indicated in units of Airy distance ( $\lambda/D$ ).
- 5.1.6.** For each image reported as part of the milestone demonstration, the average contrast recorded within the area spanning  $2 - 8 \lambda/D$ .
- 5.1.7.** For each image reported as part of the milestone demonstration, the average contrast recorded within the area spanning  $2 - 3 \lambda/D$ .
- 5.1.8.** A description of the data reduction algorithms, in sufficient detail to guide an independent analysis of the delivered data.
- 5.1.9.** Contrast metric values and supporting statistics for the overall data used to satisfy the milestone requirements, including a pixel-by-pixel histogram of contrast values across the dark field.

## 6. References

- Brown, R. A., Soummer, R., "New Completeness Methods for Estimating Exoplanet Discoveries by Direct Detection", *ApJ*, **715**, 122-131, (2010).
- Catanzarite, J., Shao, M., "Exo-Earth/Super-Earth Yield of JWST Plus a Starshade External Occulter", *PASP*, **123**, 171-178, 2011.
- Catanzarite, J., Shao, M., "The Occurrence Rate of Earth Analog Planets Orbiting Sunlike Stars", <http://arxiv.org/abs/1103.1443v1>, 2011.
- Clampin, M., et. al., "Extrasolar Planetary Imaging Coronagraph (EPIC)", *Proc. SPIE 6265*, 2006.
- Crepp, J. R., et. al., "Speckle Suppression with the Project 1640 Integral Field Spectrograph", *ApJ*, **729**, 132, 2011.
- Guyon, O., "Imaging Faint Sources within a Speckle Halo with Synchronous Interferometric Speckle Subtraction", *ApJ*, **615**, 562, (2004).
- Hinkley, S., et. al., "A New High Contrast Imaging Program at Palomar Observatory", *PASP*, **123**, 74-86, 2011.
- Lyon, R.G., Clampin, M., Woodruff, R.A., Vasudevan, G., Thompson, P., Petrone, P., Madison, T., Rizzo, M., Melnick, G., Tolls, V., "Visible nulling coronagraph testbed results", *Proc. SPIE 7440*, 744011 (2009).
- Marois, C., Lafreniere, D., Doyon, R., Macintosh, B., Nadeau, D., "Angular Differential Imaging: a Powerful High-Contrast Imaging Technique", *ApJ*, **641**, 556, (2006).
- NRC (National Research Council), "New Worlds, New Horizons in Astronomy and Astrophysics", <http://www.nap.edu/catalog/12951.html>, 2010
- Postman, M., et. al., "ADVANCED TECHNOLOGY LARGE-APERTURE SPACE TELESCOPE (ATLAST): A TECHNOLOGY ROADMAP FOR THE NEXT DECADE", [http://www.stsci.edu/institute/atlast/documents/ATLAST\\_NASA\\_ASMCS\\_Public\\_Report.pdf](http://www.stsci.edu/institute/atlast/documents/ATLAST_NASA_ASMCS_Public_Report.pdf) (Appendix K) (2009).
- Pueyo, L., et. al., "Application of a Damped locally Optimized Combination of Images Method to the Spectral Characterization of Faint Companions Using an Integral Field Spectrograph", *ApJ Supplement Series*, **199**, 6, 2012
- Rao, S.R., Wallace, J. K., Samuele, R., Chakrabarti, S., Cook, T., Hicks, B., Jung, P., Lane, B., Levine, B.M., Mendillo, C., Schmidtlin, E., Shao, M., and Stewart, J., "Path length control in a nulling coronagraph with a MEMS deformable mirror and a calibration interferometer", *Proc. SPIE 6888*, 68880B (2008).
- Samuele, R., Wallace, J. K., Schmidtlin, E., Shao, M., Levine, B. M., and Fregoso, S., "Experimental Progress and Results of a Visible Nulling Coronagraph", *Aerospace Conference, 2007 IEEE*, vol., no., pp.1-7, 3-10 March 2007.
- Savransky, D., Kasdin, N. J., Cady, E., "Analyzing the Designs of Planet-Finding Missions", *PASP*, **122**, 401-419, 2010.
- Serabyn, E., "Nulling Interferometry: Symmetry Requirements and Experimental Results", *SPIE Vol 4006*, 328-339, 2000.
- Shao, M., et. al., "DAVINCI: Dilute Aperture Visible Nulling Coronagraphic Imager, ASTRO2010 Request for Information White Paper #36", [http://sites.nationalacademies.org/BPA/BPA\\_049855](http://sites.nationalacademies.org/BPA/BPA_049855), 2009

- Trauger, J.T., Traub, W.A., "A laboratory demonstration of the capability to image an Earth-like extrasolar planet", *Nature*, 446, 771 (2007).
- Vasisht, G., Crossfield, I.J., Dumont, P.J., Levine, B.M., Troy, M., Shao, M., Shelton, J.C., Wallace, J.K., "Post-Coronagraph Wavefront Sensing for the TMT Planet Formation Imager", *Proc. SPIE 6272*, 627253 (2006).
- Wallace, J.K., Angione, J., Bartos, R., Best, P., Buruss, R., Fregoso, S., Levine, B.M., Nematy, B., Shao, M., Shelton, C., "Post-Coronagraph Wavefront Sensor for Gemini Planet Imager," *Proc. SPIE 7015*, 70156N (2008).
- Wallace, J. K., Bartos, R., Rao, S., Samuele, R., Schmidtlin, E., "A Laboratory Experiment for Demonstrating Post-Coronagraph Wave Front Sensing and Control for Extreme Adaptive Optics," *Proc. SPIE 6272*, 62722L (2006).
- Wallace, J.K., Macintosh, B., Shao, M., Bartos, R., Dumont, P., Levine, B.M., Rao, S., Samuele, R., Shelton, C., "An Interferometric Wave Front Sensor for Measuring Post-Coronagraph Errors on Large Optical Telescopes," *Aerospace Conference, 2007 IEEE E*, vol., no., pp.1-7, 3-10 March 2007.

## 7. Acronyms

<b>Acronym</b>	<b>Explanation</b>
APEP	Visible Nuller Coronagraph testbed at JPL
DAViNCI	Dilute Aperture Visible Nulling Coronagraphic Imager
DM	Deformable mirror
EPIC	Extrasolar Planetary Imaging Coronagraph
IWA	Inner Working Angle
OAP	Off-Axis Parabola
VNC	Visible Nulling Coronagraph